

## Testing the resolving power of two-dimensional $K^+K^+$ interferometry

Sandra S. Padula and Cristiane G. Roldão

*Instituto de Física Teórica, Universidade Estadual Paulista, Rua Pamplona 145, CEP 01405-900 São Paulo, Brazil*

(Received 26 May 1998)

We show results from an analysis performed to test the resolving power of a two-dimensional  $\chi^2$  method proposed previously when applied to the case of kaon interferometry, where no significant contribution from long-lived resonances is expected. For that purpose, use is made of the preliminary E859  $K^+K^+$  interferometry data from Si+Au collisions at 14.6A GeV/c. Although less sensitivity is achieved in the present case, this analysis seems to favor scenarios with no resonance formation at the AGS energy range. The possible compatibility of data with zero decoupling proper time interval, conjectured by the three-dimensional experimental analysis, is also investigated and is ruled out when considering more realistic dynamical models with expanding sources. Furthermore, these results strongly emphasize that the static Gaussian parametrization cannot be trusted under more realistic conditions, leading to a distorted or even wrong interpretation of the source parameters. [S0556-2813(98)03711-X]

PACS number(s): 25.75.Gz, 25.75.Dw

### I. INTRODUCTION

The second-order interferometry of identical particles is a powerful tool for probing the space-time zone from which they were emitted [1]. Almost two decades ago, it was suggested as a possible signature of the quark gluon plasma (QGP), expected to be formed in high-energy nucleus-nucleus collisions, by probing the expected large space-time dimensions of the emitting system at freeze-out. About ten years ago, when the first O+Au runs from CERN/SPS became available, there were expectations that we could be seeing its formation, particularly from  $\pi\pi$  interferometry [2]. However, because of limited statistics, the correlation function at that time had to be projected in one dimension only, leading to ambiguity in describing the overall behavior of interferometry data; i.e., they could be equally well described by two very distinct freeze-out scenarios [3]. One of them reflected a dynamical model in which the pions were formed after the hadronization of the QGP and the other one considered, instead, the formation of a hadronic gas of resonances.

On the other hand, several studies [4–6] have shown that dynamical models considering expanding systems would lead to effects that could dramatically distort the two-particle correlation function. Among them, the most significant effect [4] was caused by long-lived resonances, which later decayed into the observed particles. As a side consequence of this study, it was suggested to use pion interferometry to probe resonance formation at energies where their fractions were unknown [7]. Once again ambiguity in separating different scenarios emerged, evidencing symptoms of urgency for very accurate and high-statistics data, which has become available more recently, allowing for multidimensional analyses. Nevertheless, together with improved data, more precise theoretical and phenomenological tests were required, leading to the method suggested in Ref. [8], in which a two-dimensional  $\chi^2$  analysis was proposed to study the resolving power of pion interferometry. For that purpose, two dynamical scenarios were considered which predicted similar correlation functions, although the underlying decou-

pling geometries differed considerably. In one, long-lived resonances were neglected, while in the other a resonance gas with fractions predicted by the Lund model [9] was considered.

In order to stress and quantify the differences in terms of a  $\chi^2$  interferometric analysis, the contribution of long-lived resonances decaying into pions seemed to be essential. This fact led to the question of whether the resolving power of the method would remain high under less favorable conditions, i.e., if only shorter-lived resonances would contribute to the particle yield, as is the case in  $K^+K^+$  interferometry. This is precisely the goal of this paper. Furthermore, the method is also applied to test the hypothesis of the zero time emission interval, suggested by the experimental fit using three-dimensional (3D) static Gaussian parametrization [10]. In this study the influence of the time emission interval on the transverse radius parameter emerged naturally and another very important point was clearly emphasized; i.e., the static Gaussian parametrization, popularly used to fit data, is usually misleading in more realistic situations and results in a distorted or even wrong interpretation of the source parameters. Prior to reaching these points, however, we present a brief summary of the theoretical model underlying the analysis, the so-called covariant current ensemble formalism [4,11], and a brief review of the method discussed in Ref. [8]. This is then adapted to the present case, in which use is made of the preliminary E859 bidimensional data on  $K^+K^+$  interferometry from AGS/BNL.

### II. COVARIANT CURRENT ENSEMBLE FORMALISM

Under idealized conditions the correlation function  $C_2(k_1, k_2)$  of two identical bosons probes their decoupling or freeze-out space-time distribution  $\rho(x)$  through  $C_2(k_1, k_2) = 1 + |\rho(k_1 - k_2)|^2$ . However, in actual high-energy reactions, final-state interactions, correlations between coordinate and momentum variables, and resonance production distort this ideal interference pattern, corresponding only to Bose-Einstein symmetry (see, e.g., [3–6]). This may lead to an erroneous interpretation about the underlying information on

the decoupling geometry coming from the second-order interference pattern. In realistic cases, then, it is mandatory to employ more general formalisms [3–6,11], flexible enough to include such nonideal effects, reflecting model-dependent scenarios. In the covariant current ensemble formalism, the correlation function can be expressed as [4,11]

$$C(k_1, k_2) = Y(q) \left( 1 + \frac{|G(k_1, k_2)|^2}{G(k_1, k_1)G(k_2, k_2)} \right), \quad (2.1)$$

where  $Y(q) = (q_c/q)/(e^{q_c/q} - 1)$  is the Gamow factor that distorts the interference pattern due to final-state Coulomb interactions, with  $q_c = 2\pi\alpha m$  and  $q = [-(k_1 - k_2)^2]^{1/2}$ .

In general, when resonances are produced, the complex amplitude  $G(k_1, k_2)$  can be written as

$$G(k_1, k_2) \approx \left\langle \sum_r f(K^+/r) (1 - iqu_r/\Gamma_r)^{-1} \times e^{iqx_r} j_0^*(u_f^\mu k_{1\mu}) j_0(u_f^\mu k_{2\mu}) \right\rangle, \quad (2.2)$$

where  $f(K^+/r)$  is the fraction of the observed  $K^+$ 's arising from the decay of a resonance of type  $r$ , which freezes out with final four-velocity  $u_r^\mu$ . It should be noted that, in the absence of resonances, the sum in Eq. (2.2) reduces to only one term  $f(K^+) = 1$ . The currents  $j_0(u_f^\mu k_i)$  contain information about the production dynamics.

The ensemble average in the above notation is performed by using the following parametrization for the implicit breakup distribution [3,4]:

$$D(x, p) \propto \tau \exp \left\{ -\frac{\tau^2}{\Delta\tau^2} - \frac{(y-y^*)^2}{2Y_c^2} - \frac{(\eta-y)^2}{2\Delta\eta^2} - \frac{x_T^2}{R_T^2} \right\} \times \delta(E - E_p) \delta^2(p_T), \quad (2.3)$$

where  $\tau = (t^2 - z^2)^{1/2}$  is the freeze-out proper time, and  $\eta = \frac{1}{2} \ln[(t+z)/(t-z)]$  and  $y = \frac{1}{2} \ln[(E+p_z)/(E-p_z)]$  are the space-time and momentum rapidity variables, respectively. The correlation between these rapidities is estimated from the Lund model to be  $\Delta\eta \approx 0.8$  [4],  $Y_c = 0.7$ , and  $y_{c,m}^* = 0$ . As regarding resonance fractions, the Lund model [9] in the

AGS range suggests essentially two contributions for that scenario, i.e., that  $f(K_{\text{direct}}^+) = 0.5$ ,  $f(K^+/K^*) = 0.5$ .

We should notice that in Eq. (2.3) the parameter  $\Delta\tau$  determines both the mean emission time  $\langle\tau\rangle \propto \Delta\tau$  and the width of the emission time distribution. If we were to compare with the more general case in which the proper-time distribution would be proportional to  $\exp[-(\tau - \tau_0)^2/\Delta\tau^2]$ , and consequently  $\langle\tau\rangle = \langle\tau(\tau_0, \Delta\tau)\rangle$ , the parametrization in Eq. (2.3) would still be applicable to cases where  $\Delta\tau$  dominates the contribution to the mean  $\langle\tau\rangle$  as, for instance, for  $\Delta\tau \gg \tau_0$  or  $\Delta\tau = \tau_0$ , besides the obvious case in which  $\tau_0 = 0$ . In such situations, prolonged emission would be associated with sources whose mean  $\langle\tau\rangle$  would also be big and sudden emitting sources to those with small  $\langle\tau\rangle$ . However, the case corresponding to a source with a small duration of particle emission (small width  $\Delta\tau$ ) and a large mean emission time ( $\tau_0 \gg \Delta\tau$ ) would definitely be excluded by the time distribution in Eq. (2.3). This last case, however, will not be considered in the present analysis.

We recall that the transverse momentum in the more general model proposed in Ref. [4] is assumed to arise entirely from the finite momentum spread  $\Delta p$  of the pion wave packets. It should also be clarified that this model coincides with the covariant current ensemble formalism in the case of minimum packets, when associating the momentum spread to the so-called pseudotemperature  $T_{\text{PS}}$  through  $\Delta p^2/m = T_{\text{PS}}$ . This pseudothermal ansatz, however, was previously used in order to derive an analytical form for the correlation function [11]. In the present analysis we are basically considering the covariant current ensemble formalism but, since numerical calculations are carried out from the start, we consider the full thermal ansatz instead, in which  $T$  is the effective inverse transverse mass slope from the experimental fit, i.e.,  $T = 0.18$  GeV [12], corresponding to an average momentum  $\langle k_T \rangle \approx 0.49$  GeV/c. It should be added that no clear difference could be seen when comparing the correlation functions corresponding to the thermal versus pseudothermal cases, in the same kinematical region. The currents in the thermal model may be written covariantly as  $j_0(k) = \sqrt{u^\mu k_\mu} e^{-u^\mu k_\mu/2T}$ .

By carrying out the ensemble average in Eq. (2.2) with the aid of Eq. (2.3) and of  $j_0(k)$  defined above, we obtain the expressions for  $G(k_1, k_2)$  used in the numerical calculations:

$$G(k_1, k_2) \propto e^{-q_T^2 R_T^2/4} \int_0^\infty \tau d\tau e^{-\tau^2/\Delta\tau^2} \int_{-\infty}^{+\infty} dy e^{-(y-y^*)^2/2Y_c^2} \int_{-\infty}^{+\infty} d\eta e^{-(\eta-y)^2/2\Delta\eta^2} e^{i\tau(q_0 \cosh \eta - q_L \sinh \eta)} \times \sum_r f(K^+/r) (1 - iqu_r/\Gamma_r)^{-1} \sqrt{[m_{1r} \cosh(y_r - y_1)][m_{2r} \cosh(y_r - y_2)]} \exp\{-m_{1r} \cosh(y_r - y_1)/2T\} \times \exp\{-m_{2r} \cosh(y_r - y_2)/2T\}. \quad (2.4)$$

The single inclusive kaon distribution in this notation is  $P_1(k_i) \propto G(k_i, k_i)$ , which can be written, with the help of Eq. (2.3), as

$$G(k_i, k_i) \propto \int_0^\infty \tau d\tau e^{-\tau^2/\Delta\tau^2} \int_{-\infty}^{+\infty} dy e^{-(y-y^*)^2/2Y_c^2} \int_{-\infty}^{+\infty} d\eta e^{-(\eta-y)^2/2\Delta\eta^2} \sum_r f(K^+/r) [m_{1r} \cosh(y_r - y_i)] \times \exp\{-m_{1r} \cosh(y_r - y_i)/T\}. \quad (2.5)$$

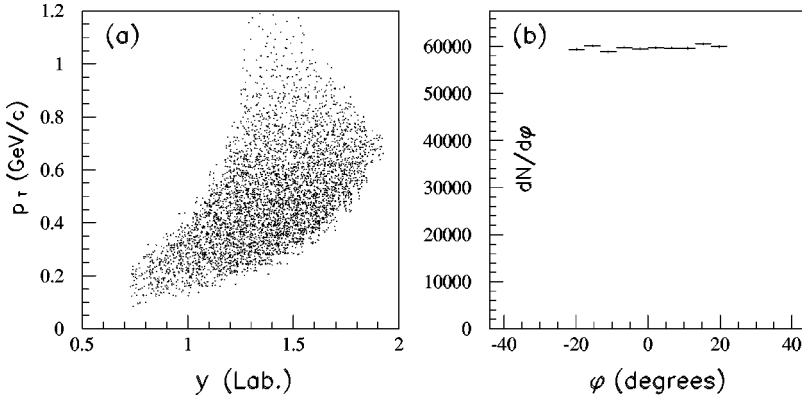


FIG. 1. Phase space generated by the CERES code, with the simplified cuts shown in Eqs. (3.2) and (3.3). In part (a) we see the generated transverse momenta versus rapidity; part (b) shows the generated azimuthal angle distribution.

The aim of the present study is to test if multidimensional kaon interferometry can discriminate scenarios including resonances from those in which they are absent, even in the much less striking limit of no significant long-lived resonance contribution to the kaon yield. For doing this, we apply the method suggested in Ref. [8] to extract the rms transverse radius  $R_T$  at decoupling and the rms decoupling proper time interval  $\Delta\tau$ . Note that we assume implicitly that the chaoticity parameter  $\lambda = 1$  throughout our analysis.

### III. $\chi^2$ ANALYSIS

To compare theoretical correlation functions with data projected onto two of the six dimensions, we must compute the projected correlation function as

$$C_{\text{proj}}(q_T, q_L) = \frac{\int d^3k_1 d^3k_2 P_2(k_1, k_2) A_2(q_T, q_L; k_1, k_2)}{\int d^3k_1 d^3k_2 P_1(k_1) P_1(k_2) A_2(q_T, q_L; k_1, k_2)}, \quad (3.1)$$

where  $P_1$  and  $P_2$  are the one- and two-kaon inclusive distributions, and  $A_2$  is the experimental two-kaon binning and acceptance function. All calculations were performed using the Monte Carlo importance sampling method adopted in the CERES code [4].

The acceptance function for the E859 experiment was approximated [10] by

$$A_2(q_T, q_L; k_1, k_2) = A_1(k_1) A_1(k_2) \Theta(22 - |\phi_1 - \phi_2|) \times \delta(q_L - |k_{1z} - k_{2z}|) \delta(q_T - |k_{1T} - k_{2T}|). \quad (3.2)$$

The angles are measured in degrees and the momenta in GeV/c. The single inclusive distribution cuts are specified by

$$A_1(k) = \Theta(14 < \theta_{\text{lab}} < 28) \times \Theta(p_{\text{lab}} < 2.9 \text{ GeV/c}) \Theta(y_{\text{min}} > 0.75). \quad (3.3)$$

It can be seen from Fig. 1 that the phase space generated with the above cuts reproduces very closely that covered by

the experiment [10]. Only a few excess generated particles can be seen at low transverse momentum  $p_T$  (or  $k_{iT}$ ).

To assess the statistical significance of the differences between the fits obtained assuming resonance and nonresonance dynamics, we computed the  $\chi^2$  goodness of fit, estimating this variable as previously [8,13]:

$$\chi^2(i, j) = \frac{[A(i, j) - \mathcal{N}_\chi^{-1} C_{\text{th}}(i, j) B(i, j)]^2}{\{[\Delta A(i, j)]^2 + [\mathcal{N}_\chi^{-1} C_{\text{th}}(i, j) \Delta B(i, j)]^2\}}, \quad (3.4)$$

where  $\mathcal{N}_\chi$  is a normalization factor which is chosen to minimize the average  $\chi^2$  and depends on the range in the  $(q_T, q_L)$  plane under analysis. The indices  $i, j$  refer to the corresponding  $q_T, q_L$  bins, in each of which the experimental correlation function is given by

$$C_E(i, j) = \mathcal{N}_\chi \frac{A(i, j)}{B(i, j)},$$

$$\Delta C_E(i, j) = C_E(i, j) \sqrt{\left(\frac{\Delta A(i, j)}{A(i, j)}\right)^2 + \left(\frac{\Delta B(i, j)}{B(i, j)}\right)^2}. \quad (3.5)$$

The numerator  $A(i, j) \pm \Delta A(i, j)$  and denominator  $B(i, j) \pm \Delta B(i, j)$  in Eqs. (3.4) and (3.5) were obtained from Cianciolo [10,12], understanding that the data in this form are preliminary and subject to further final analysis. Use is made of their preliminary form mainly for testing the sharpness of the method. Note that in the present analysis we are not including the errors associated with the theoretical correlation function generated by the Monte Carlo importance sampling in CERES. All calculations, however, were performed by taking high-statistics runs only, making it reasonable to consider those errors as negligible.

Analogously to the procedure adopted in Ref. [8], minimization of the average  $\chi^2$  was performed by exploring the parameter space of  $R_T$  and  $\Delta\tau$  and computing the  $\langle \chi^2 \rangle$ , averaging over a grid of nearly  $30 \times 30$  bins in the  $(q_T, q_L)$  plane in the relative momentum region  $0.005 < q_T, q_L < 0.605$  GeV/c, binned with  $\delta q_T = \delta q_L = 0.02$  GeV/c. A very meticulous investigation was performed to find the most probable region where the minimum  $(R_{T_0}, \Delta\tau_0)$  could be located.

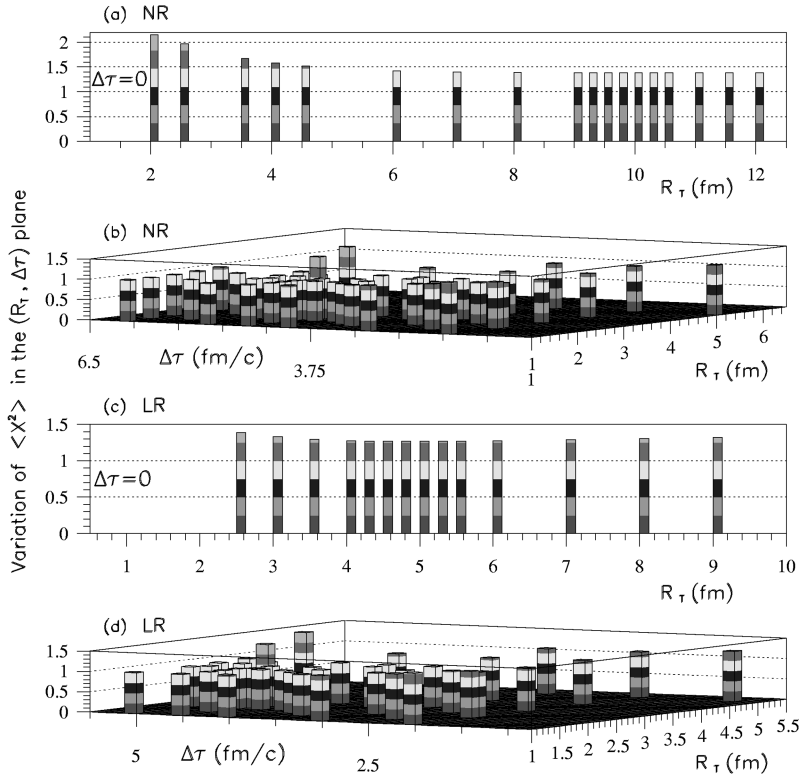


Figure 2 illustrates most of the investigated region in the  $(R_T, \Delta\tau)$  plane. Parts (a) and (c) will be discussed later. In the vicinity of the minimum, the parameters of the quadratic surface  $\langle \chi^2(R_T, \Delta\tau) \rangle = \chi_{\min}^2 + \alpha(R_T - R_{T_0})^2 + \beta(\Delta\tau - \Delta\tau_0)^2$  were determined. The results of such an investigation are given in Table I, where the radius parameters are measured in fm and time intervals in fm/c.

The errors appearing in Table I were estimated following the prescription of Ref. [8], which considered the  $\chi^2$  over  $N$  bins as a random variable and, for large  $N$ , approximated the distribution of the mean  $\chi^2$  per bin by  $P(\chi^2) \propto \exp[-(\chi^2 - 1)^2/2\sigma^2]$ , with rms width  $\sigma = \sqrt{2/N} \approx 0.048$ , for the  $N=855$  grid under consideration (i.e., subtracting from the original 900 the empty bins and the number of degrees of freedom consumed in the  $\chi^2$  analysis itself). Inserting the

TABLE I. Two-dimensional  $\chi^2$  analysis of kaon decoupling geometry.

$\chi^2(R_T, \Delta\tau)$	No res. ( $f_{K_{\text{dir}}}=1$ )	LUND res. ( $f_{K_{\text{dir}}}=f_{K/K^*}=0.5$ )
Optimized $R_T$ and $\Delta\tau$		
$\langle \chi_{\min}^2 \rangle_{30 \times 30}$	1.03	1.02
$\langle \chi_{\min}^2 \rangle_{10 \times 10}$	1.17	1.30
$R_{T_0}$	$2.19 \pm 0.76$	$1.95 \pm 0.89$
$\Delta\tau_0$	$4.4 \pm 2.0$	$4.4 \pm 2.6$
$\alpha$	0.0410	0.0299
$\beta$	0.0058	0.0034
Optimized $R_T(\Delta\tau=0)$		
$\langle \chi_{\min}^2 \rangle_{30 \times 30}$	1.29	1.33
$\langle \chi_{\min}^2 \rangle_{10 \times 10}$	4.04	2.92
$R_{0_T}$	$\sim 10.6$	$\sim 4.8$
$\alpha$	0.0003	0.0280

FIG. 2. Zone in the  $(R_T, \Delta\tau)$  plane investigated, leading to the determination of the most probable region where the minimum  $\langle \chi^2 \rangle$ , associated with  $(R_T, \Delta\tau)$ , could be located. Part (b) corresponds to the dynamics ignoring the contribution of  $K^*$  and part (d) to including their contribution to the kaon yield. Similarly, parts (a) and (c) correspond to nonresonance and resonance cases, respectively, but fixing  $\Delta\tau=0$  and optimizing only  $R_T$ .

expression for  $\langle \chi^2(R_T, \Delta\tau) \rangle$  in the above paraboloid into the asymptotic form of the  $\chi^2$  distribution for large  $N$ , the likelihood for the parameter  $R_T$  to have a value near the minimum is approximately  $\propto \exp[-\alpha^2(R_T - R_{T_0})^4/2\sigma^2]$ . Therefore the estimated error in the radius is  $\Delta R \approx \{\sqrt{2}[\Gamma(3/4)/\Gamma(1/4)]\sigma/\alpha\}^{1/2} \approx 0.7(\sigma/\alpha)^{1/2}$ , and similarly the error on the proper time interval is  $0.7(\sigma/\beta)^{1/2}$ .

Comparing Table I with Ref. [8], we may see that the optimized value of  $\Delta\tau$ , the decoupling time interval, is estimated to be about the same as in the pion case. However, the transverse size of the kaon emission region seems to be half that of the pions. This result agrees with the experimental fit to the data and, as was stated in Ref. [10], it could be reinforcing the suggestion given in Ref. [14], according to which kaons could decouple earlier than pions due their small cross section for interacting with nuclear matter.

We see from Table I that the optimization in both scenarios results in similar values for  $\langle \chi^2 \rangle$  over 855 bins, although using the optimized parameters we see smaller  $\langle \chi^2 \rangle$  for the non-resonance scenario in a smaller  $(10 \times 10)$  grid. Just to illustrate the similarities, we can see in Fig. 3 the two-dimensional correlation functions  $C(q_T, q_L)$ , corresponding to data and to the theoretical values generated with the optimized values shown in Table I.

From the above discussion, similarly to what happened in the pion case, we see that not enough separation is found, neither from the 2D projection alone, nor by conjugating it to the average  $\chi^2$  analysis. However, in Ref. [8] it has already been recalled that a most direct measure of the goodness of fit could be achieved by means of  $n_\sigma = |\langle \chi_{\min}^2 \rangle - 1|/\sigma$ , the number of standard deviations from unity of the average  $\chi^2$  per degree of freedom. Since  $n_\sigma$  depends on the range of  $q$  under analysis, we followed the steps of Ref. [8] and studied its behavior by varying the range of the analysis to restricted

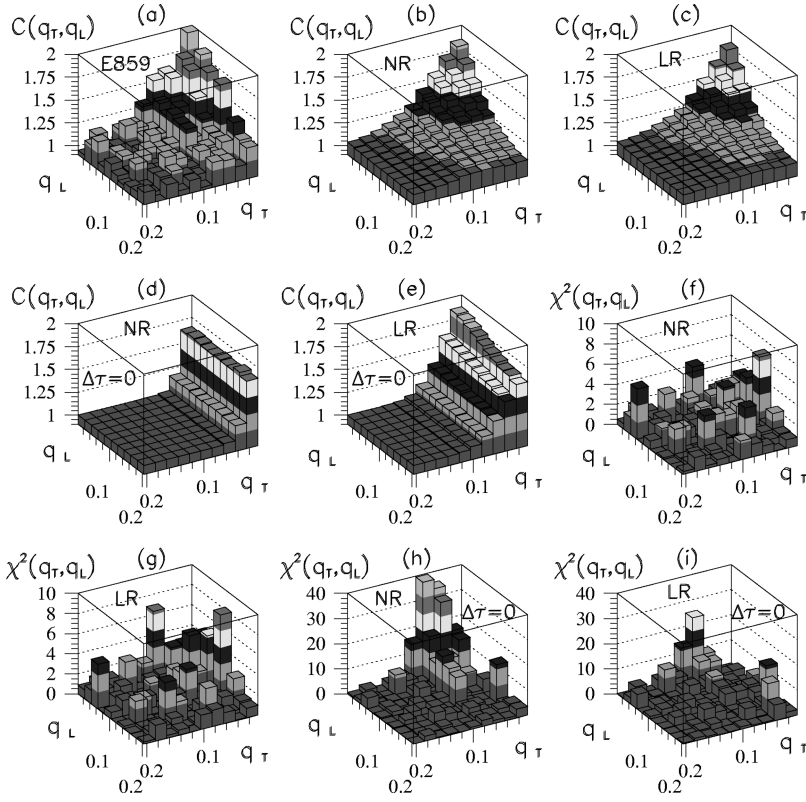


FIG. 3. The preliminary E859 Gamow corrected data are shown in part (a);  $q_T$  and  $q_L$  are the pair momenta differences (in GeV/c) in the transverse and longitudinal directions, respectively. Part (b) shows theoretical correlation functions  $C(q_T, q_L)$ , filtered with the E859 acceptance for the case with no resonances (NR) and part (c) refers to the inclusion of Lund resonance (LR) fractions; the corresponding distribution of  $\chi^2(q_T, q_L)$  are in (f) and (g), respectively. Similarly, when fixing  $\Delta\tau=0$ , results for the generated  $C(q_T, q_L)$  are shown in parts (d) (NR) and (e) (LR), with the  $\chi^2(q_T, q_L)$  distribution in (h) and (i), respectively.

$(q_T, q_L)$  domain, ranging from a  $2 \times 2$  grid, corresponding to  $0.025 < q_T, q_L < 0.045$  GeV/c, to  $3 \times 3$ ,  $4 \times 4$ , etc., as shown in Fig. 4. For each  $n \times n$  grid,  $N = n^2$  is the number of degrees of freedom and the standard deviation is expected to be  $\sigma = \sqrt{2/n}$ . The strong dependence of the number of standard deviations from unity as a function of the range of the analysis is brought out clearly in Fig. 4.

Although less striking than in the pion case, we see from Fig. 4 that it still is possible to separate the two scenarios, although none of them could be considered as a very good fit. This situation could become better in the near future with improving statistics, which could allow for smaller bin sizes. It is clear, however, that the nonresonance picture is closer to the preliminary data in the entire range significant for interferometry, i.e., in the smaller domain  $q_T, q_L < 0.20$  GeV/c, where the correlation function deviates significantly from unity. The two models yield similar fits in terms of  $\chi^2$  for  $q_{\max} > 200$  MeV/c because in that large domain both models trivially predict nearly unit correlation functions.

In Fig. 4(b) two curves signaled with  $\Delta\tau=0$  can be seen.

This result corresponds to fixing the decoupling time interval to zero (instantaneous freeze-out) and searching for the optimized value of  $R_T$ . This test was performed following a suggestion in Ref. [10], according to which the preliminary 3D experimental analysis in  $q_0, q_T, q_L$  returned results for  $R_T, R_L$  compatible with values obtained by the 2D analysis, although the value of  $\Delta\tau$  found could either be  $\Delta\tau \approx R_T$  or  $\Delta\tau = 0$ . We should recall that the experimental analysis had to project data in large bins (width of 180 MeV) [10] in order to have enough statistics in the time direction which, by itself, could be responsible for dramatically weakening the interferometric signal. However, that ambiguous conclusion regarding the time interval was reached when a static Gaussian space-time parametrization was used in the experimental fit. We then decided to test what would be the response of the method to it, since we consider a different class of models, in which the longitudinal expansion is taken into account. The region of  $R_T$  searched in its optimization, keeping  $\Delta\tau=0$ , is shown in Figs. 2(a) and 2(c). The optimized values for  $R_T$  are shown in Table I. The errors, estimated with the

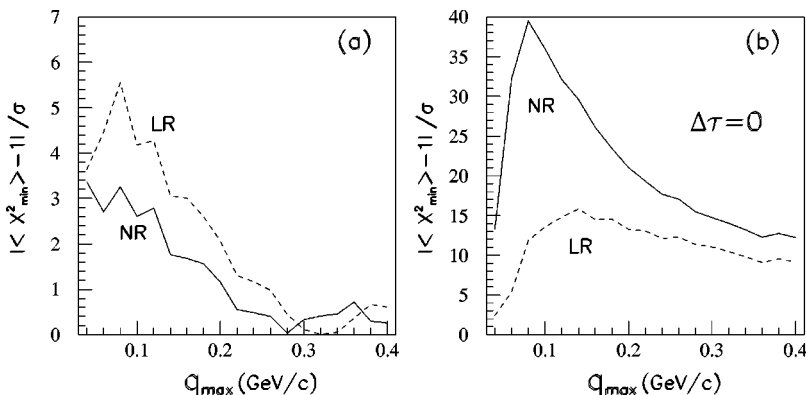


FIG. 4. Number of standard deviations of  $\langle \chi^2 \rangle$  from unity for increasing number of bins. In part (a),  $R_T$  and  $\Delta\tau$  were optimized, whereas in (b), only  $R_T$  was.

aid of the asymptotic form of the  $P(\chi^2)$  distribution, would not apply to this case. The reason is that, for considering the average  $\chi^2$  over  $N$  bins as a random variable with unit mean and rms width  $\sigma = \sqrt{2/N}$ , as discussed above, the  $\chi(i, j)$  should be normal random variables with zero mean and unit rms width. We estimated this distribution in each case by running CERES for the optimized values. When fixing  $\Delta\tau$  to be zero, however, the assumption made about the  $\chi(i, j)$  distribution was not verified. For this reason, we prefer to simply show the optimized values of  $R_T$  as approximate ones. The corresponding results can be seen both in Figs. 3(d) and 3(e) [with corresponding  $\chi^2$  in (h) and (i), respectively], as well as in Fig. 4(b). From this last one, we see that our model completely excludes instantaneous emission. In particular, even in the region where no correlation is expected (roughly for  $q_T, q_L > 200$  MeV), the deviation with respect to data continues to be enormous.

Furthermore, the above analysis nicely illustrates the important and well-known [4–6] influence of the time spread in the *effective* transverse radius  $R_T$ . Although its influence would be noticeable even for a static Gaussian parametrization of the space-time decoupling geometry [4], models considering expanding systems strengthen the effect [4,5]. In the present analysis, the time influence on  $R_T$  can be inferred from the fact that the optimized radius increases considerably, trying to compensate for the strong constraint of the zero emission time interval. For instance, when including the  $K^*$  contribution, its finite lifetime tries to circumvent the problem by introducing a nonzero time spread through the resonance decay; albeit the optimized  $R_T$  is about twice the value without that constraint. This effect is, however, more dramatic in the nonresonance case, where no clear evidence about the location of the optimized value of  $R_T$  can be seen from Fig. 2(a), since there is no way out to accommodate the instant emission constraint.

We conclude that the multidimensional analysis proposed in Ref. [8], which has high resolving power in the domain of

physical interest in the case of pion interferometry, can still be applied to the case of kaon interferometry, although with less resolving power, due to the absence of contributions from long-lived resonances. Besides, the results seem to indicate the absence of resonance formation at the AGS energy range, in agreement with the previous one involving pions [8]. Naturally, this conclusion is valid only within the class of models considered by the present analysis. Finally, the above two-dimensional  $\chi^2$  analysis indicates that, as far as the preliminary E859 data are concerned, expanding sources should be considered at the AGS energy range, since expansion enhances the influence of the emission time interval on the transverse dimensions of the source and, from the present analysis, kaon sources emitting instantaneously are discarded. This should also be considered as a warning against the common practice of employing the static Gaussian parametrization to fit data since, by using it, the interpretation of the corresponding extracted parameters could be misleading or even wrong. After the completion of the present work we became aware of similar warnings in Ref. [15], where the authors show that the radii parameters obtained through the so-called Gaussian *model-independent* formulation of Hanbury Brown–Twiss effect (HBT) [16] are, in general, “qualitatively as well quantitatively unreliable for systems with long-lived resonances.”

#### ACKNOWLEDGMENTS

We are very grateful to V. Cianciolo for making his unpublished data files and analysis available to us, and to W. Zajc and R. Soltz for many illustrative discussions. Helpful comments from M. Gyulassy and several discussions with P. Gouffon, M. C. Gonzalez-Garcia, and R. Vazquez on practical matters are also thankfully acknowledged. This work was partially supported by Conselho Nacional de Desenvolvimento Científico e Tecnológico (CNPq) and Fundação de Amparo à Pesquisa do Estado de São Paulo (FAPESP), Brazil.

- 
- [1] W. A. Zajc, *Hadronic Multiparticle Production*, edited by P. Carruthers (World Scientific, Singapore, 1988); D. H. Boal, C. K. Gelbke, and B. K. Jennings, *Rev. Mod. Phys.* **62**, 553 (1990); C-Y. Wong, *Introduction to High-Energy Heavy-Ion Collisions* (World Scientific, Singapore, 1994).
  - [2] NA35 Collaboration, A. Bamberger *et al.*, *Phys. Lett. B* **203**, 320 (1988).
  - [3] Miklos Gyulassy and Sandra S. Padula, *Phys. Lett. B* **217**, 181 (1989).
  - [4] Sandra S. Padula, M. Gyulassy, and S. Gavin, *Nucl. Phys.* **B329**, 357 (1990); Sandra S. Padula and M. Gyulassy, *ibid.* **B339**, 378 (1990).
  - [5] Yojiro Hama and Sandra S. Padula, *Phys. Rev. D* **37**, 3237 (1988).
  - [6] S. Pratt, *Phys. Rev. D* **33**, 1314 (1986); G. Bertsch, M. Gong, and M. Tohyama, *Phys. Rev. C* **37**, 1896 (1988); T. Csörgö and J. Zimanyi, *Nucl. Phys.* **A527**, 621c (1991); S. Chapman, J. R. Nix, and U. Heinz, *Phys. Rev. C* **52**, 2694 (1995); T. Csörgö and B. Lörstad, *Nucl. Phys.* **A590**, 465 (1995); U. Heinz, B. Tomasik, U. A. Wiedermann, and Y. F. Wu, *Phys. Lett. B* **382**, 181 (1996).
  - [7] Sandra S. Padula and M. Gyulassy, *Nucl. Phys.* **A525**, 339c (1990).
  - [8] Sandra S. Padula and Miklos Gyulassy, *Phys. Lett. B* **348**, 303 (1995).
  - [9] B. Andersson, G. Gustafson, and B. Nilsson-Almqvist, *Nucl. Phys.* **B281**, 289 (1987); M. Gyulassy, in *Proceedings of the Eighth Balaton Conference on Nuclear Physics*, edited by Z. Fodor, KFKI, Budapest, 1987, Report No. CERN-TH-4794, 1987.
  - [10] Y. Akiba *et al.*, *Phys. Rev. Lett.* **70**, 1057 (1993); O. E. Vossnack, *Nucl. Phys.* **A566**, 535c (1994); V. Cianciolo, *ibid.* **A590**, 459c (1995).
  - [11] M. Gyulassy, S. K. Kaufmann, and L. W. Wilson, *Phys. Rev. C* **20**, 2267 (1979); K. Kolehmainen and M. Gyulassy, *Phys. Lett. B* **180**, 203 (1986).
  - [12] V. Cianciolo (private communication).
  - [13] W. Zajc, in *Proceedings of CAMP (LESIP IV)*, edited by M.

- Plümer, S. Raha, and R. M. Weiner (World Scientific, Singapore, 1991), p. 439.
- [14] S. Schnetzer, M. C. Lemaire, R. Lombard, E. Moller, S. Nagamiya, G. Shapiro, H. Steiner, and I. Tanihata, Phys. Rev. Lett. **49**, 989 (1982).
- [15] S. Nickerson, T. Csörgö, and D. Kiang, Phys. Rev. C **57**, 3251 (1998).
- [16] S. Chapman, P. Scotto, and U. Heinz, Heavy Ion Phys. **1**, 1 (1995).